

## Supplementary Materials for

### Deuterium metabolic imaging (DMI) for MRI-based 3D mapping of metabolism in vivo

Henk M. De Feyter\*, Kevin L. Behar, Zachary A. Corbin, Robert K. Fulbright, Peter B. Brown, Scott McIntyre, Terence W. Nixon, Douglas L. Rothman, Robin A. de Graaf\*

\*Corresponding author. Email: [henk.defeyter@yale.edu](mailto:henk.defeyter@yale.edu) (H.M.D.F.); [robin.degraaf@yale.edu](mailto:robin.degraaf@yale.edu) (R.A.d.G.)

Published 22 August 2018, *Sci. Adv.* **4**, eaat7314 (2018)  
DOI: 10.1126/sciadv.aat7314

#### This PDF file includes:

Fig. S1. DMI of [6,6'-<sup>2</sup>H<sub>2</sub>]glucose and [<sup>2</sup>H<sub>3</sub>]acetate metabolism.

Fig. S2. High-resolution <sup>1</sup>H NMR of rat plasma.

Fig. S3. DMI detects the effect of DCA on glucose metabolism.

Fig. S4. Difference in <sup>2</sup>H-acetate metabolism between normal-appearing rat brain and tumor tissue.

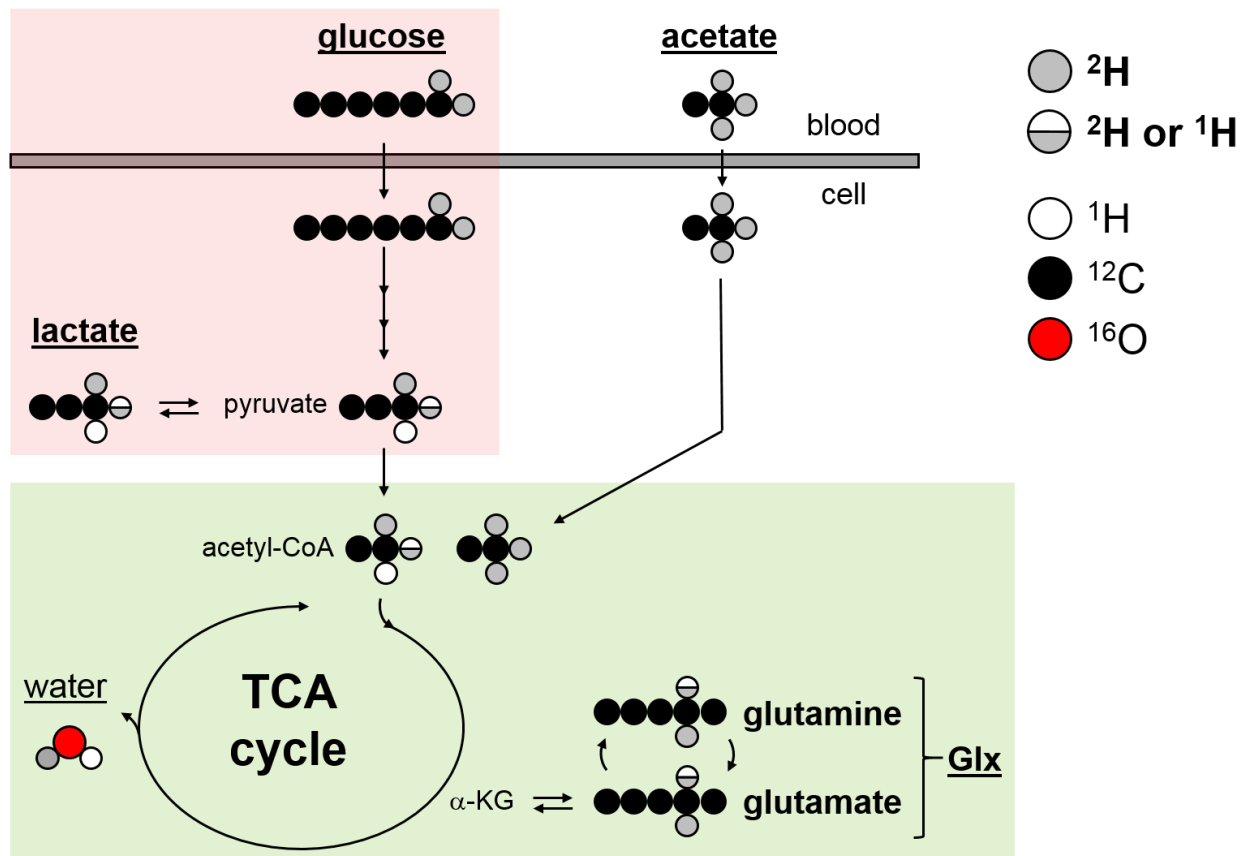
Fig. S5. In vivo <sup>2</sup>H MRSI spectra from human brain.

Fig. S6. DMI of the Warburg effect in a patient with GBM.

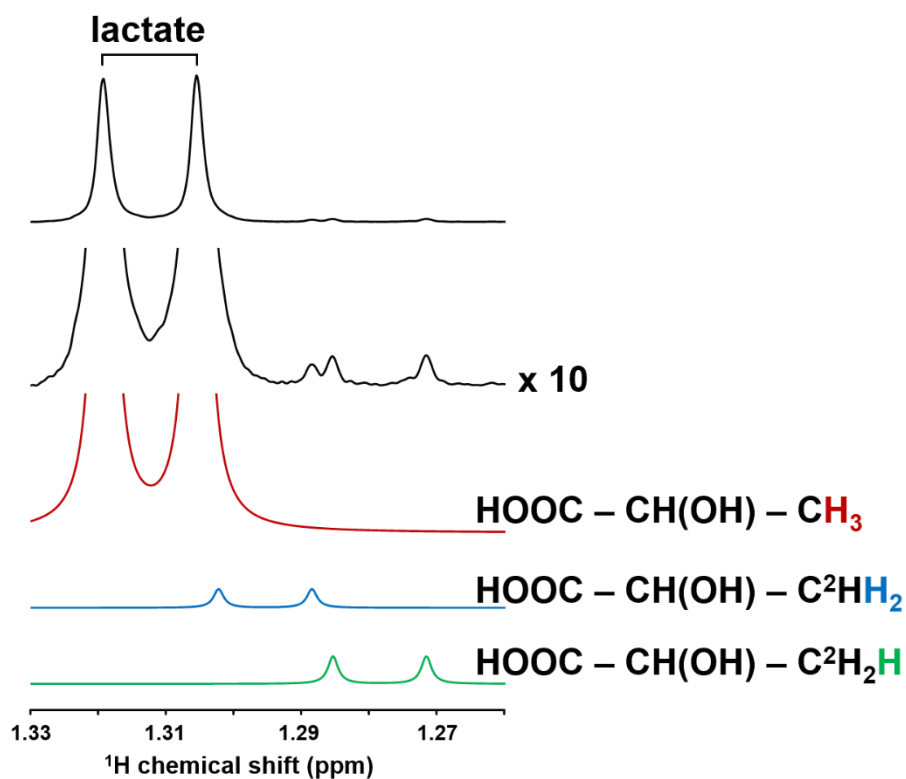
Fig. S7. High-resolution <sup>13</sup>C NMR spectra of <sup>13</sup>C- and <sup>2</sup>H-labeled lactate in cell culture medium.

Table S1. T<sub>1</sub> and T<sub>2</sub> relaxation times.

Table S2. T<sub>2</sub>\* of water from the brain in vivo at 4 and 11.7 T.



**Fig. S1. DMI of  $[6,6'\text{-}^2\text{H}_2]$ glucose and  $[^2\text{H}_3]$ acetate metabolism.** Schematic illustrating the metabolism of  $^2\text{H}$ -label from  $[6,6'\text{-}^2\text{H}_2]$ -glucose and  $[^2\text{H}_3]$ -acetate. Only relevant  $^2\text{H}$  and  $^1\text{H}$  atoms are shown. After entering the cell, glucose is metabolized in the glycolytic pathway (red-shaded background), which has pyruvate as the end-product. Pyruvate can either be converted to lactate or enter the mitochondria (green-shaded background) for complete oxidation in the tricarboxylic acid (TCA) cycle. Oxidation of glucose or acetate results in glutamate and glutamine labeling through rapid exchange with the TCA-cycle intermediate  $\alpha$ -ketoglutarate ( $\alpha$ -KG). During formation of citrate, one proton from the acetyl-CoA methyl group is removed. In the case of  $^2\text{H}$ -labeled acetyl-CoA, the citrate formation can therefore result in loss of the  $^2\text{H}$  label, illustrated by the mixed color of the  $^1\text{H}/^2\text{H}$  symbol. The label loss during citrate formation gives rise to two labeled species of glutamate and glutamine, with one or two  $^2\text{H}$  atoms:  $[4,4'\text{-}^2\text{H}_2]$  and  $[4\text{-}^2\text{H}]$ . The metabolites readily observed with DMI are glucose, acetate, lactate and glutamate+glutamine (Glx). When combined with  $[6,6'\text{-}^2\text{H}_2]$ -glucose administration, DMI reveals glucose uptake and both glycolytic and oxidative metabolism in a single acquisition. If DMI is used with acetate infusion, both acetate uptake and oxidation can be observed.



**Fig. S2. High-resolution  $^1\text{H}$  NMR of rat plasma.** Example of a  $^2\text{H}$ -decoupled  $^1\text{H}$  NMR spectrum of protein-free plasma from a rat infused with  $[6,6'\text{-}^2\text{H}_2]$ -glucose, showing the lactate methyl resonance at 1.313 ppm. The zoomed in region (x 10) shows how the resonances are shifted by the  $^2\text{H}$ - $^1\text{H}$  J-coupling while the concomitant peak splitting has been nullified by  $^2\text{H}$  decoupling. The chemical shift induced by  $^2\text{H}$ - $^1\text{H}$  J-coupling on the  $^1\text{H}$  resonance is -0.017 ppm for  $[3\text{-}^2\text{H}]$ -lactate and -0.034 ppm for  $[3,3'\text{-}^2\text{H}_2]$ -lactate. The individual components of the spectral fit are indicated in colors matching the chemical formula of the different lactate species shown on the right. These data allow to determine the  $^2\text{H}$  fractional enrichment of plasma lactate and calculate the concentration of  $^2\text{H}$ -labeled lactate in plasma.

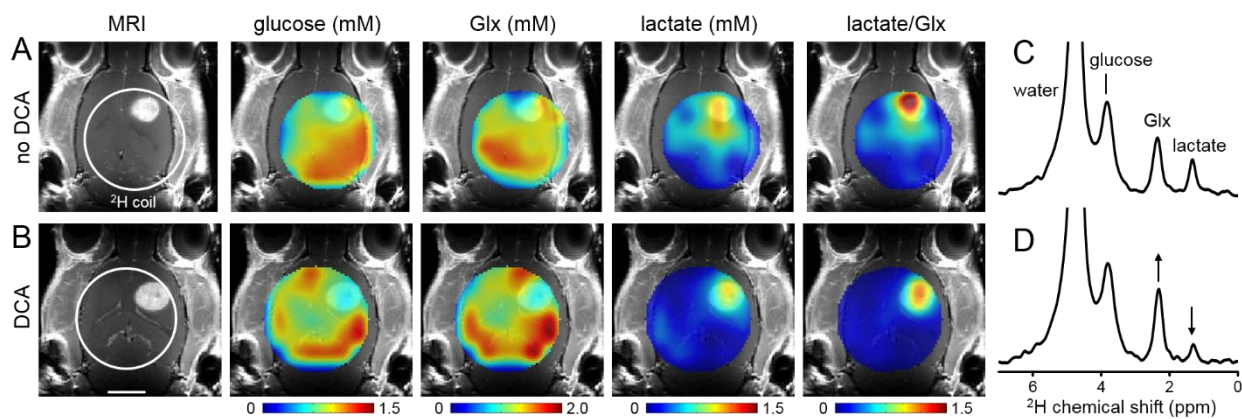


**Fig. S3. DMI detects the effect of DCA on glucose metabolism.** Contrast-enhanced  $T_1$ -weighted MRI and color-coded DMI maps of glucose and metabolites acquired in an RG2-bearing rat. Data were acquired 60-90 min after the start of intraperitoneal  $[6,6'\text{-}^2\text{H}_2]$ -glucose infusion, on two consecutive days, A) without and B) with dichloroacetate treatment (DCA, 200 mg/kg). DCA's stimulatory effect on pyruvate dehydrogenase results in higher levels of labeled Glx and lower levels of lactate. The effect of DCA, seen in the DMI maps of labeled Glx and lactate, generates an apparently smaller region of less intense lactate/Glx, consistent with a partial reversal of the Warburg effect. (C, D) The effects of DCA on both Glx and lactate labeling could also be observed in non-localized  $^2\text{H}$  NMR spectra acquired in 1 min.

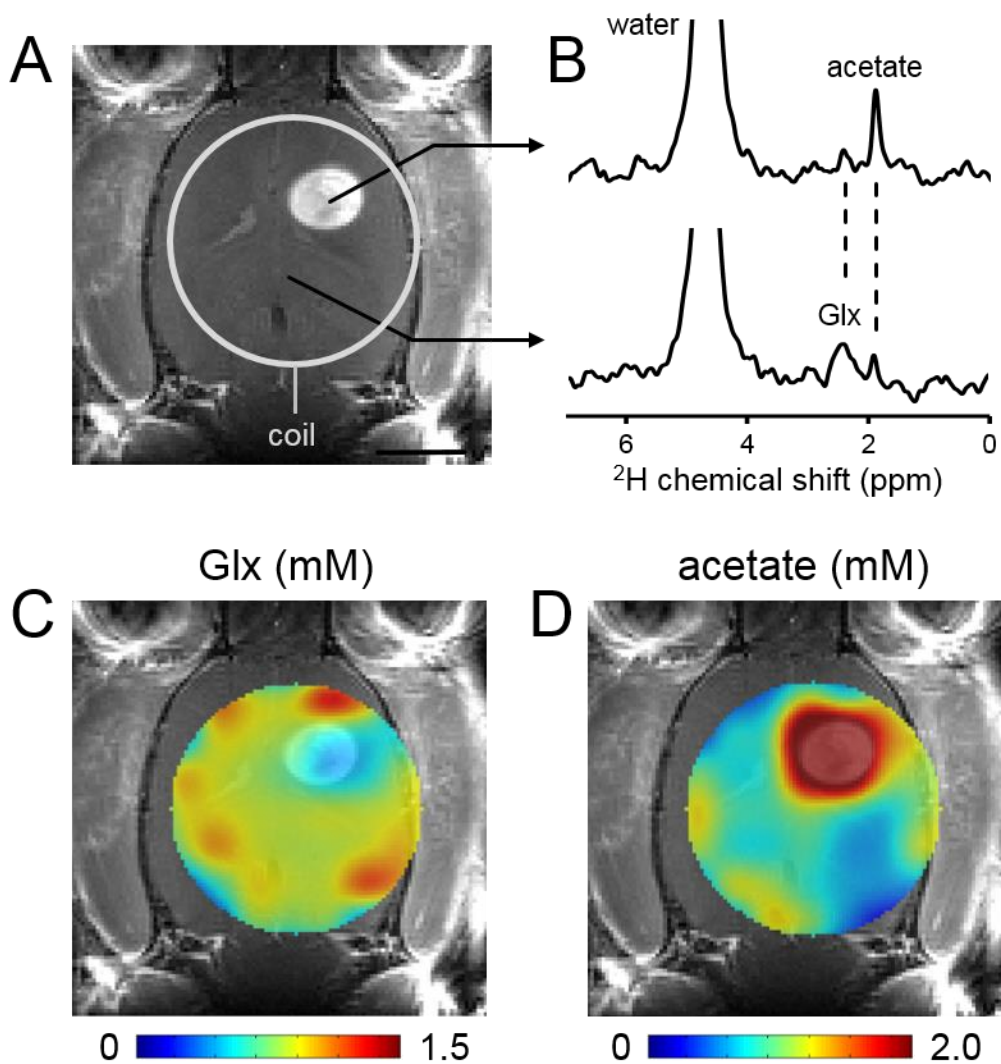


**Fig. S4. Difference in  $^2\text{H}$ -acetate metabolism between normal-appearing rat brain and tumor tissue.** A)  $T_1$ -weighted, contrast-enhanced MRI of glioma-bearing rat and the extent of the  $^2\text{H}$  surface coil. Scale bar = 5 mm. B)  $^2\text{H}$  MR spectra extracted from  $^2\text{H}$  MRSI data originating from the tumor lesion (top) and normal-appearing brain (bottom). DMI maps showing the lower concentration of labeled Glx in the tumor (C) and noticeable contrast resulting from the high level of labeled acetate in the tumor (D).

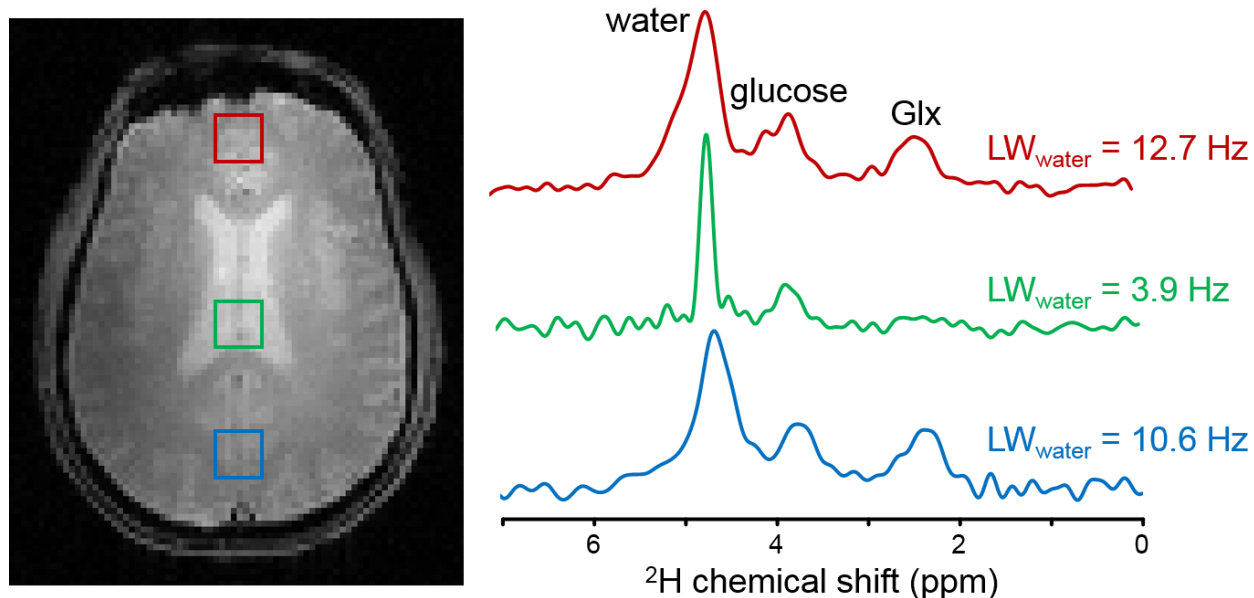


**Fig. S5. In vivo  $^2\text{H}$  MRSI spectra from human brain.** Individual  $^2\text{H}$  NMR spectra selected from the 3D MRSI dataset from the frontal lobe (top, in red), cerebrospinal fluid (middle, in green) and the occipital lobe (bottom, in blue). Comparing the spectra from frontal lobe (top, in red) and occipital lobe (bottom, in blue) shows the minimal deterioration of quality due to magnetic field inhomogeneity as is typically seen in  $^1\text{H}$  MR spectra acquired in the frontal lobe. Further, note the narrow linewidths of the water and glucose peaks, and lack of Glx signal in the  $^2\text{H}$  NMR spectrum acquired from the cerebrospinal fluid of the ventricles in the center of the brain.

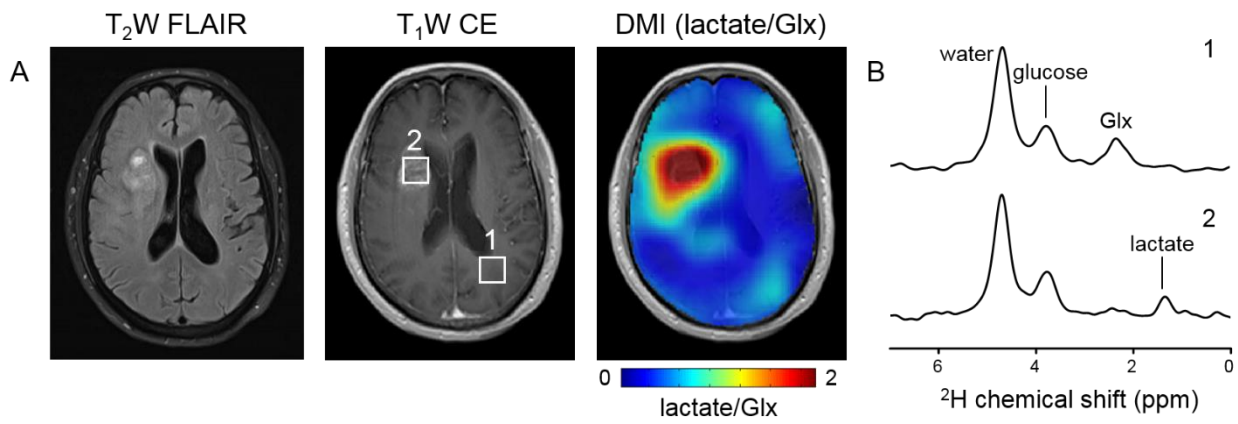


**Fig. S6. DMI of the Warburg effect in a patient with GBM.** A) Clinical MR images acquired as standard of care in a patient diagnosed with GBM in the right frontal lobe, T<sub>2</sub>-weighted fluid-attenuated inversion recovery (T<sub>2</sub>W FLAIR), T<sub>1</sub>-weighted contrast-enhanced imaging (T<sub>1</sub>W CE), and T<sub>1</sub>W MRI with overlaid map of DMI showing lactate/Glx. DMI data were acquired between 75 and 105 minutes after oral intake of [6,6'-<sup>2</sup>H<sub>2</sub>]-glucose. Note the strong contrast generated by differences in glucose metabolism in the tumor lesion area compared to the rest of the brain, similar to the data shown in Fig. 4. B) Individual <sup>2</sup>H NMR spectra selected from regions depicted on T<sub>1</sub>W CE MRI shown in (A).

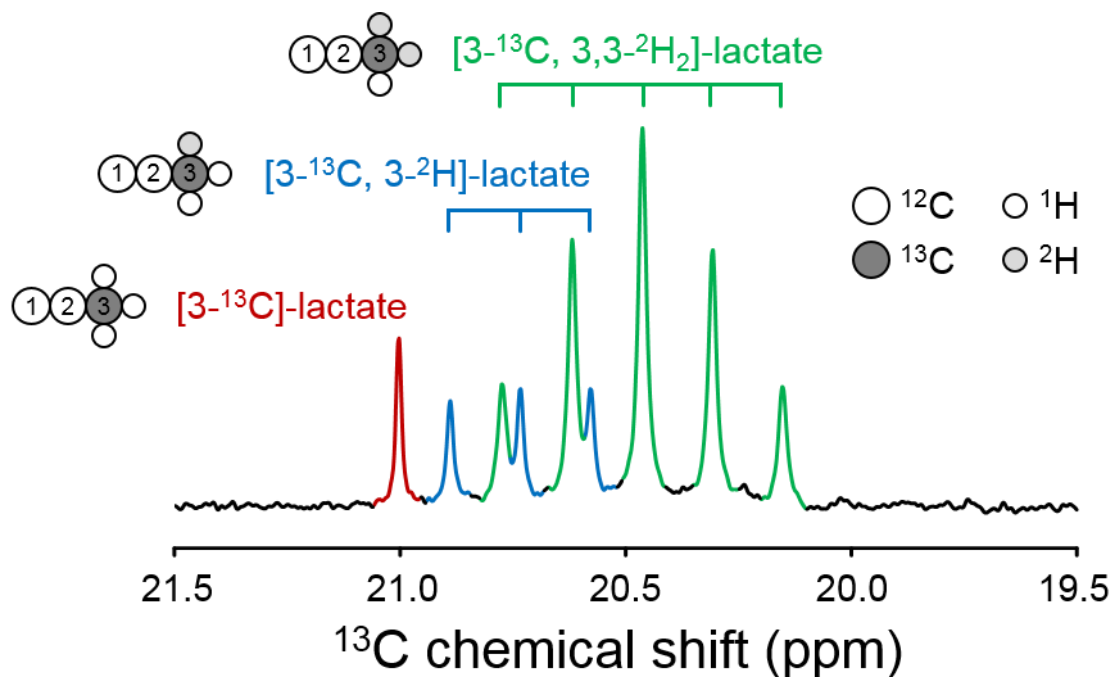


**Fig. S7. High-resolution  $^{13}\text{C}$  NMR spectra of  $^{13}\text{C}$ - and  $^2\text{H}$ -labeled lactate in cell culture medium.**  $^{13}\text{C}$ ,  $^1\text{H}$ -decoupled NMR spectrum of lactate acquired in concentrated cell culture media of 9L glioma cells, after 6 hrs of incubation with unlabeled glucose and [6- $^{13}\text{C}$ ,6,6'- $^2\text{H}_2$ ]-glucose. The cell culture medium does not contain lactate before incubation, instead the lactate is produced through glycolysis by the 9L cells.  $^{13}\text{C}$ - $^2\text{H}$  J-coupling induces both a shift and a splitting of the adjacent  $^{13}\text{C}$  resonances, which allows to discriminate 3 species of lactate: [3- $^{13}\text{C}$ ]-lactate, [3- $^{13}\text{C}$ ,3- $^2\text{H}$ ]-lactate and [3- $^{13}\text{C}$ ,3,3'- $^2\text{H}_2$ ]-lactate. The [3- $^{13}\text{C}$ ]-lactate originates from the unlabeled glucose in the medium, the unlabeled triose of the [6- $^{13}\text{C}$ ,6,6'- $^2\text{H}_2$ ]-glucose (C1,2,3), and from the  $^2\text{H}$ -labeled triose of the [6- $^{13}\text{C}$ ,6,6'- $^2\text{H}_2$ ]-glucose that lost its  $^2\text{H}$ -label. Quantitative analysis of these incubation experiments (n=3) indicate the total  $^2\text{H}$  loss during glycolysis to be  $8.1 \pm 2.3$  %.



**Table S1. T<sub>1</sub> and T<sub>2</sub> relaxation times.**

		4T			11.7T		
	Resonance	T <sub>1</sub> (ms)	T <sub>2</sub> (ms)	Fraction (%)	T <sub>1</sub> (ms)	T <sub>2</sub> (ms)	Fraction (%)
<i>In vivo</i>	Water, fraction 1	346 ± 5	26 ± 1	82 ± 4	320 ± 28	12 ± 2	65 ± 13
	Water, fraction 2	-	351 ± 51	18 ± 4	-	31 ± 4	35 ± 13
	Glucose	67 ± 11	42 ± 1	-	64 ± 2	32 ± 2	-
	Glx	139 ± 11	44 ± 3	-	146 ± 11	32 ± 5	-
	Lactate	n.a.	n.a.	-	297 ± 61	61 ± 27	-
<b>Post mortem</b>	Water, fraction 1	n.a.	n.a.	n.a.	257 ± 46	14 ± 2	37 ± 14
	Water, fraction 2	n.a.	n.a.	n.a.	-	31 ± 2	63 ± 14
	Glx	n.a.	n.a.	n.a.	126 ± 5	44 ± 8	-
	Lactate	n.a.	n.a.	n.a.	262 ± 23	80 ± 3	-
<b>Phantom</b>	Water	446 ± 7	372 ± 17	-	462 ± 9	334 ± 21	-
	Glucose in water	59 ± 2	59 ± 4	-	60 ± 1	57 ± 1	-
	Water + 1.5% agarose	340 ± 20	69 ± 4	-	409 ± 4	81 ± 1	-
	Glucose in water + 1.5% agarose	52 ± 1	52 ± 4	-	56 ± 1	50 ± 1	-

<sup>2</sup>H T<sub>1</sub> and T<sub>2</sub> values (mean ± standard deviation in ms) determined in human brain at 4T (n=2) and rat brain at 11.7T (n=3) after administration of [6,6'-<sup>2</sup>H<sub>2</sub>]-glucose. Lactate values were determined from data acquired post mortem in situ. The two fractions of water T<sub>2</sub> reflect the two time constants of the bi-exponential fitting procedure for T<sub>2</sub>. No bi-exponential relaxation was observed in phantoms. This is in agreement with the hypothesis of intracellular and extracellular compartmentalized water seen in vivo, that is not replicated by adding agarose in phantoms. Note the strong effect on the water T<sub>2</sub> induced by adding agarose to the solution. Glx = glutamate + glutamine; n.a.= not available; - = not applicable.

**Table S2. T<sub>2</sub>\* of water from the brain in vivo at 4 and 11.7 T.**

<b>Water T<sub>2</sub>*</b>	<b>4T</b>	<b>11.7T</b>
<b>Min</b>	11.2 ± 1.5	10.7 ± 1.1
<b>Max</b>	90.2 ± 11.9	43.0 ± 9.4
<b>Mean</b>	32.8 ± 12.3	22.7 ± 6.8

Minimum, maximum and mean T<sub>2</sub>\* values (mean ± standard deviation in ms) derived from peak linewidths of deuterium-labeled water from individual voxels of 3 DMI studies in human brain at 4T and 3 DMI studies in rat brain at 11.7T. The number of voxels analyzed for the 3 human studies were 165, 194 and 178. The number of voxels analyzed for the 3 rat studies were 66, 62 and 59.